RESEARCH ARTICLE

Society For Biomaterials | WILEY

Elastic modulus of hydrogel regulates osteogenic differentiation via liquid–liquid phase separation of YAP

Kuang Tan[1,2] | Qiaolin Yang[1,2] | Yineng Han[1,2] | Ziyao Zhuang[1,2] | Yi Zhao[1,2] | KunYao Guo[1,2] | Anqi Tan[1,2] | Yunfei Zheng[1,2] | Weiran Li[1,2]

[1]Department of Orthodontics, Peking University School and Hospital of Stomatology, Beijing, China

[2]National Center for Stomatology; National Clinical Research Center for Oral Diseases, National Engineering Laboratory for Digital and Material Technology of Stomatology, Beijing, China

Correspondence
Yunfei Zheng and Weiran Li, Department of Orthodonitcs, Peking University School and Hospital of Stomatology, No.22, Zhongguancun South Avenue, Haidian District, Beijing 100081, PR China.
Email: yunfei_zheng@bjmu.edu.cn and weiranli@bjmu.edu.cn

Abstract

Craniofacial bone defects induced by congenital malformations, trauma, or diseases frequently challenge the orthodontic or restorative treatment. Stem cell-based bone regenerative approaches emerged as a promising method to resolve bone defects. Microenvironment physical cues, such as the matrix elastic modulus or matrix topography, regulate stem cell differentiation via multiple genes. We constructed gelatin methacryloyl (GelMA), a well-known scaffold, to investigate the impact of elastic modulus on osteogenic differentiation in a three-dimensional environment. Confocal microscope was used to observe and assess the condensates fission and fusion. New bone formation was evaluated by micro-computed tomography at 6 weeks in calvarial defect rat. We found that the light curing increased elastic modulus of GelMA, and the pore size of GelMA decreased. The expression of osteogenic markers was inhibited in hBMSCs cultured in the low-elastic-modulus GelMA. In contrast, the expression of YAP, TAZ and TEAD was increased in the hBMSCs in the low-elastic-modulus GelMA. Furthermore, YAP assembled via liquid–liquid phase separation (LLPS) into condensates that were sensitive to 1′6-hexanediol. YAP recruit TAZ and TEAD4, but not RUNX2 into the condensates. In vivo, we also found that hBMSCs in high-elastic-modulus GelMA was more apt to form new bone. This study provides new insight into the mechanism of osteogenic differentiation. Reagents that can regulate the elastic modulus of substrate or LLPS may be applied to promote bone regeneration.

KEYWORDS
GelMA, hBMSCs, LLPS, osteogenic differentiation, YAP

1 | BACKGROUND

Defect in alveolar bone caused by congenital or pathological reason frequently make the orthodontic therapy complicated. Specifically, alveolar bone grafting is needed for patients with cleft alveolus and cleft palate since the following orthodontic treatment requires the continuity of bone bridge.[1] Autografting is the well-recognized choice to repair the defect. However, bone autografts are always insufficient and not reliable.[2] Stem cell based bone regeneration is an alternative option to provide solution to bone defect.[3] Human bone marrow-derived stem cells (hBMSCs) possess the ability to differentiate into multiple lineages including osteoblasts, make them attractive for clinical applications.[4] The fate of hBMSCs were regulated by not only the biological signals but also the mechanical signals of culture substrates.[5,6] The elastic modulus of culturing substrates was found to affect the fate of stem cells in a reliable and precise way.[7] Manipulating the mechanical micro-circumstances of cell culturing is promising to improve the differentiation of hBMSCs.[8]

Recently, membrane less biomolecular condensates that formed via liquid–liquid phase separation (LLPS) have been shown to regulate the

wileyonlinelibrary.com/journal/jbma

biological events in cells. LLPS sequester macromolecules within a compartment, or increases their local concentration, thereby facilitating molecular interactions.[9] LLPS drives nonspecific binding of biomacromolecules and has accelerated a targeted search for downstream molecules, reducing the search space and accelerating diffusion kinetics.[10,11] Temperature, ionic strength, and molecular concentration affect LLPS.[12,13] During LLPS, scaffold molecules are the subject of phase-separated liquids. Client molecules participate differently depending on the ratio and valency of scaffold molecules.[13] Intrinsically disordered regions (IDRs) of proteins are enriched in phase-separated compartments and may be a diagnostic index of phase-separation ability of the protein.[14]

Yes-associated protein (YAP), a crucial component of the Hippo pathway, mediates mechanosensing signaling during extracellular matrix-cell interactions. YAP controls tissue growth, organ size, tumorigenesis,[15] and cell differentiation.[16] Recently, YAP was found to condensate through LLPS and involved in tumor development and cell differentiation. For example, YAP self-congregates and phase separates into condensates to regulate re-organized genome topology under hyperosmotic conditions or on the stimulation by cytokines (such as interferon-γ) to induce tumor resistance.[17,18] Crowding agents, such as PEG-8000, Ficoll, or Dextran, also induce YAP LLPS.[19,20] YAP contained several IDRs, including the domains of TEAD-binding (TB), WW, coiled-coiled (CC), and transcription activation (TA), are important for YAP condensates formation.[19]

The role of YAP in osteogenic differentiation is controversial. YAP activation reportedly enhances osteogenesis by regulating β-catenin signaling, and also essential for osteoclastogenesis via a TEAD-dependent mechanism.[21–23] YAP has multiple domains that bind transcription factors. For example, the TB domain binds TEAD and RUNX.[19,24] TEAD family transcription factors are evolutionarily conserved key mediators of YAP biological functions, including tumorigenesis in cancer cells.[25] RUNX genes are molecular switches coordinating the developmental balance between proliferation and differentiation.[24] YAP and TAZ are paralogues with similar domain structures and partially overlapping functions, are similarly regulated by Hippo kinases, and collaboratively function in multiple responses.[26]

Gelatin methacryloyl (GelMA), a derivative of gelatin, is a famous hydrogel for bone regeneration due to its bioactivity, good biocompatibility and biodegradability, and tunable mechanical strength. In the present study, we investigated the effect of substrate elasticity on YAP LLPS and the role of YAP LLPS in regulating osteoblast differentiation using GelMA. Scaffolds of varying elastic modulus were constructed and we investigated the role and mechanism of YAP LLPS in osteoblast differentiation. We found that a low-elastic-modulus GelMA promoted YAP LLPS, recruiting TAZ and TEAD4, but not RUNX2, to inhibit osteogenic differentiation.

2 | MATERIALS AND METHODS

2.1 | Cell culture

hBMSCs were purchased from ScienCell Company (San Diego, USA). All cell experiments were performed in triplicates. Cells were cultured in minimum essential medium α (α-MEM, Gibco, USA), 10% fetal bovine serum (FSS500, ExCell Bio, China), and 1% penicillin/streptomycin (15070063, Gibco, USA). Cells were cultured at 37°C in a humidified incubator with 5% CO_2. hBMSCs with passage numbers between 3 and 7 were used in all cell experiments, and plated at $\sim 10^6/cm^3$.

2.2 | Construction of three-dimensional (3D) GelMA

GelMA was purchased from Yongqinquan Intelligent Equipment Co., Ltd. (EFL-GM-60, Engineering for Life, China). We selected a 60% (from 30%, 60%, 90%) grafting yield of GelMA (GM60). One gram photo initiator was dissolved in 20 mL sterile phosphate-buffered saline (PBS, AQ10010, Aoqing Biotechnology, China), formed 5% final concentration, and GelMA was mixed with 5% photo initiator in a 55°C water bath. Hydrogel solution was passed through a 0.22 μm filter, and mixed with cell pellet digested with trypsin–EDTA solution (25200-072, Gibco, USA). After curing under 405 nm light (EFL-LS-1601-405, Engineering for Life, China) for 16, 19, 22, 25, or 30s. Cells were uniformly encapsulated in GelMA. All hydrogels were completely crosslinked.

2.3 | Preparation of GelMA samples for scanning electron microscopy (SEM)

Five groups of GelMA samples were molded and stored at −80°C overnight. Frozen samples were lyophilized for ~24 h and examined by SEM (Zeiss EVO18, Germany) after metal spraying. Pore length was analyzed by Image J software ($n = 3$ per group, and 15 pores were selected randomly in each image).

2.4 | Preparation of GelMA samples for analysis of physical and chemical properties

2.4.1 | Elastic modulus

200 μL of GelMA solution injected into a 14 mm round mold and cured for 16, 19, 22, 25, and 30s respectively ($n = 3$). Cured GelMA samples were transferred to a universal tensile testing machine (Instron, 5969, UK) for compression testing. The stress–strain curve was recorded and the first 10% slope of the strain on curve was taken as its elastic modulus.

2.4.2 | Fourier transform infrared (FTIR) spectroscopy

GelMA samples were vacuum-dried overnight and mixed with potassium bromide powder. In the range of 4000–0 cm^{-1} wavenumbers, FTIR spectroscopy (Thermos, Nicolet-6700) was performed in ATR mode via potassium bromide pressing.

2.4.3 | Swelling ratio

Cured GelMA samples were soaked in PBS, and weighed at 5, 15, 30 min, 1, 2, 6, 24, and 48 h after removing surface water (W1). Samples were vacuum dried and weighed (W2). Swelling ratio = $(W1 − W2)/W2 \times 100\%$ ($n = 3$ per group).

2.4.4 | Degradation percent

GelMA samples was immersed in 500 μL of PBS containing 1 U mL^{-1} collagenase type II (C8150, Solarbio, Beijing) at 37°C. At 6, 12, 24, 48, and 72 h, samples were washed with deionized water to eliminate residual salts and removed surface water. After freezing and drying, samples were weighed (W2); the initial dry mass was W1. Degradation = $(W1-W2)/W1 \times 100\%$ ($n = 3$ per group).

2.5 | Cell viability assay

The Calcein-AM/Propidium Iodide (PI) Double Stain Kit (CA1630, Solarbio, Beijing) was used to assay cell viability. Briefly, cells encapsulated in GelMA were incubated with calcein-AM and PI buffer at 37°C for 30 min, washed triplicate with PBS, and immediately observed under a confocal microscope (Leica, TCS-SP8 STED 3X, Germany). Live and dead cells were enumerated using Image J software. Survival rate of hBMSCs in GelMA = $W1/(W1 + W2) \times 100\%$; W1, number of live cells; W2, number of dead cells ($n = 3$ per group).

2.6 | Cytoskeleton staining of hBMSCs

Confocal microscope (TCS-SP8 STED 3X, Leica) was used to observe the cytoskeleton of hBMSCs. According to the protocol, hBMSCs were encapsulated in GelMA and fixed in 4% paraformaldehyde (PFA, AQ201, Aoqing Biotechnology, Beijing) for 15 min at room temperature. Cells were washed three times with PBS and then blocked in 5% goat serum (ZLI-9021, ZSGB-BIO, China) for 30 min. Then the cells were stained with phalloidin (ab176753, Abcam, UK) for 1 h at room temperature. Cells were washed with PBS and nuclei were stained with DAPI (C0065, Solarbio, Beijing). The 3D morphology of cells was reconstruction by "3D" viewer. Nuclei and actin boundaries were created using an Otsu's thresholding method. The following parameters were quantified: cell volume, nucleus volume. Image analysis of confocal image was performed in LAS X software (Leica, Germany).
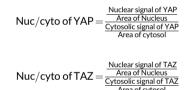
2.7 | Immunofluorescence

hBMSCs in GelMA were fixed in 4% PFA (Aoqing Biotechnology) for 15 min at room temperature and permeabilized in 0.25% (v/v) Triton X-100 (BioRuler, 9002-93-1, USA) for 10 min. Cells were washed with PBS. A block step was done in 5% goat serum (ZSGB-BIO) for 1 h. Cells

TABLE 1 Key resource table.

Recombinant DNA	Source	Identifier
pLV[Exp]-Puro-CMV > EGFP(ns):TAZ	Mijia Biotech	N/A
pLV[Exp]-Puro-CMV > EGFP(ns):TEAD4	Mijia Biotech	N/A
pLV[Exp]-Puro-CMV > mCherry(ns):YAP	Mijia Biotech	N/A
pLV[Exp]-Puro-CMV > YFP(ns):RUNX2	Mijia Biotech	N/A

incubated overnight with primary antibodies at 4°C and then washed with PBS. Cells incubated with secondary antibodies for 2 h at room temperature. Nuclei were stained with DAPI (C0065, Solarbio, Beijing). Images were captured under a confocal microscope (Leica, TCS-SP8 STED 3X). The primary antibodies used were as follows: anti-YAP (3A7A9, Proteintech, China), anti-TAZ (ab242313, Abcam, USA). The secondary antibodies used were as follows: Alexa Fluor-488 labeled goat anti-rabbit IgG(H + L) (ZF0511, ZSGB-BIO, China) and Alexa Fluor-594 labeled goat anti-mouse IgG (H + L) (ZF0513, ZSGB-BIO, China). Image analysis of confocal image was performed in LAS X software (Leica, Germany). Fluorescence intensity of the proteins of interest were quantified by "Measure" plugin. The following parameters were quantified: YAP nucleus/cytosol (nuc/cyto) ratio and TAZ nuc/cyto ratio. YAP nuc/cyto ratio and TAZ nuc/cyto ratio was calculated based on formulas below:

$$\text{Nuc/cyto of YAP} = \frac{\frac{\text{Nuclear signal of YAP}}{\text{Area of Nucleus}}}{\frac{\text{Cytosolic signal of YAP}}{\text{Area of cytosol}}}$$

$$\text{Nuc/cyto of TAZ} = \frac{\frac{\text{Nuclear signal of TAZ}}{\text{Area of Nucleus}}}{\frac{\text{Cytosolic signal of TAZ}}{\text{Area of cytosol}}}$$

2.8 | Plasmid construction and transient infection

The expression plasmid was purchased from Mijia Biotech (Beijing). YAP, TAZ, TEAD4, RUNX2, mCherry, EGFP, and YFP were subcloned into the expression vector (pLV [Exp]-Puro-CMV > shuttle). Lipofectamine 2000 (Lipo2000, 11668500, Invitrogen, USA) was used as the transfection reagent. Cells were cultured in 6-well plates with 2 mL of growth medium. The medium was exchanged for growth medium without antibiotics when cells reached ~70% confluence. Equal amounts of plasmid and Lipo2000 (w/v) were diluted in 50 μL Opti-MEM I (31985070, Gibco, USA) for 5 min at room temperature. Next, plasmid and Lipo2000 were mixed and incubated for 20 min at room temperature. The cells were transferred to a 37°C CO$_2$ incubator for 6–8 h after adding 100 μL of complexes to medium. Then the medium was exchanged for normal medium (Table 1).

2.9 | Live-cell imaging and cell treatment

Cells were imaged 24, 48, and 72 h after plasmid transfection using a confocal microscope (Leica, TCS-SP8 STED 3X) at room temperature under a plan-apochromat ×25 water objective. Images were taken at 1 s intervals to visualize the process of fission and fusion for YAP condensates. Images

were analyzed using Image J software. Colocalization analysis of two channels was performed using the "plot profile" function of Image J. 2 µg/mL Verteporfin (VP, CL318952, MedChemExpress, USA) were added to essential medium after YAP/ TAZ plasmid transfection and incubation for 48 h. Images were collected under confocal microscope (Leica).

2.10 | Fluorescence recovery after photobleaching (FRAP) assay

Cells were cultured in confocal dishes for 24 h. FRAP assay was performed in bleaching mode under a confocal microscope (Leica, TCS-SP8 STED 3X). A region of interest (ROI) was chosen in the cytoplasm or nucleus. ROI were bleached using a 562 nm laser at full power. Three and 45 imaging rounds were performed before and after bleaching until the fluorescence signal plateaued. The fluorescence intensity of selected YAP condensates at pre-bleaching and after bleaching was recorded using the microscope. The "FRAP Profiler v. 2" plugin of Image J was used to extract quantitative information and fit FRAP curves.

2.11 | Quantitative Real-time quantitative PCR (qRT-qPCR)

GelMA lysis solution (EFL-GM-LS-001, Engineering for Life, China) was used to release cells from hydrogels. Total RNA from hBMSCs was lysed using TRIzol (DP424, Tiangen, Beijing). RNA was reverse-transcription using the Evo MLV Mix Kit (AG11728, Accurate Biology, China) with cDNA Clean for Quantitative PCR (qPCR). YAP, TAZ, TEAD4, OPG, OCN, and MMP9 gene expression levels were analyzed by real-time PCR instrument (AB7500, USA) using the SYBR Green Premix PRO Taq HS Quantitative PCR Kit II (AG11719, Accurate Biology, China). The following primers were used: GAPDH, 5′-CGACAGCAGCCGCATCTT-3′ (forward) and 5′-CCAATACGACCAAATCCGTTG-3′ (reverse); YAP, 5′-TAGCCCTGCGTAGCCAGTTA-3′ (forward) and 5′-TCATGCTTAGTCCACTGTCTGT-3′ (reverse); TAZ, 5′-GTCCTACGACGTGACCGAC-3′ (forward) and 5′-CACGAGATTTGGCTGGGATAC-3′ (reverse); TEAD4, 5′-GGACACTACTCTTACCGCATCC-3′ (forward) and 5′-TCAAAGACATAGGCAATGCACA-3′ (reverse); OPG, 5′-GTGTGCGAATGCAAGGAAGG-3′ (forward) and 5′-CCACTCCAAATCCAGGAGGG-3′ (reverse); OCN, 5′-ACCCTGACCCATCTCAGAAGCA-3′ (forward) and 5′-CTTGGAAGGGTCTGTGGGGCTA-3′ (reverse); MMP9, 5′-TGTACCGCTATGGTTACACTCG-3′ (forward) and 5′-GGCAGGGACAGTTGCTTCT-3′ (reverse). mRNA levels were normalized with GAPDH.

2.12 | Western blotting

GelMA lysis solution (Engineering for Life) was used to release cells from GelMA. RIPA buffer (100 µL) (P0013B, Beyotime, Shanghai) and 1 µL of protease inhibitor cocktail (HY-K0010, MedChemExpress, USA) were added to cell pellet for 30 min in a shaker at 4°C. Lysates were

centrifuged at 12,000 $\times$ g for 30 min and the supernatants were collected. Protein concentration was determined using the BCA Kit (P0012S, Beyotime, Shanghai). Next, 5$\times$ SDS loading buffer (P1040, Solarbio, Beijing) and PBS solution was added and the complexes were boiled for 10 min. Western blot were conducted by 10% SDS-PAGE (WB2102, Biotides, Beijing) and protein samples were transferred onto polyvinylidene fluoride membranes (ISEQ00010, Millipore, USA) by wet electrophoretic transfer. Samples were incubated with primary antibody at 4°C overnight and secondary antibodies at room temperature for 1 h. The primary antibodies used were as follows: anti-YAP (Proteintech), anti-TAZ (Abcam), anti-TEAD4 (ab155244, Abcam, USA), anti-OCN (23418-1-AP, Proteintech, China), anti-OPG (sc-390,518, santa cruz, USA), anti-RUNX2 (12556S, Cell Signaling Technology, USA) anti-GAPDH (60004-1-Ig, Proteintech, China). An Imaging System (Bio-Rad) and the Gel Analysis plugin of Image J software were used to evaluate band intensities.

2.13 | Alkaline phosphatase (ALP) assay

The BCIP/ NBT ALP Color Development Kit (C3206, Beyotime, Shanghai) was used according to the manufacturer's instructions. Briefly, preparation of stain work solution and incubated cells for 30 min-1 h until cells chromogenesis. Then wash cells by ddH$_2$0 and terminate chromogenic reactions. Images were captured by upright microscope (Olympus BX60, Japan).

2.14 | Co-immunoprecipitation (Co-IP) assay

GelMA lysis solution (Engineering for Life) was used to release cells from GelMA. A Co-IP Kit (PK 10007, Proteintech, China) was used to extract protein. Briefly, 100 µL of IP lysis buffer (containing 1$\times$ protease inhibitor) was added to cells on ice for 30 min followed by centrifugation at 10,000 $\times$ g for 20 min. A 30 µL protein A Sepharose bead slurry was prepared for each sample. For cell lysis, samples in the experimental group were mixed with 2 µg of anti-YAP (Proteintech); those in the negative control group were mixed with 2 µg of control IgG (30000-0-AP, Proteintech, China). Incubation buffer (200 µL) and protein A Sepharose beads (30 µL) were incubated in spin columns overnight at 4°C. The supernatant was discarded, and the pellet was washed five times with 800 µL of 1$\times$ washing buffer. The pellet complex was eluted in 80 µL of elution buffer and mixed with 10 µL of alkali neutralization buffer and 23 µL of 5$\times$ sample buffer. Samples were boiled for 10 min and subjected to western blotting as described in Section 2.12.

2.15 | Animal experiments

2.15.1 | Establishment of a rat skull defect model and injection of hBMSCs-loaded GelMA

Animal experimental procedures were followed by the Animal Use and Care Committee of Peking University (LA2020109). A rat skull

defect model was constructed in male Sprague–Dawley rats ($\sim$ 250 g). Rats were anesthetized with 1% pentobarbital, and the surgical area was shaved and wiped with 75% alcohol. Stainless steel drill was used on both sides of the midline to create round 5 mm defects. Aseptic saline was used to flush the wound intermittently to dispel the heat generated by the drill. The rats were randomly divided into the hBMSCs-loaded GelMA (curing 30 s) ($n = 3$), hBMSCs-loaded GelMA (curing 16 s) ($n = 3$), and GelMA without hBMSCs ($n = 3$) groups.

2.15.2 | Micro-computed tomography (micro-CT)

New bone formation was evaluated at 6 weeks. Rats were executed by cervical dislocation and the cranium was fixed with 10% aldehyde fixative and subjected to micro-CT (Bruker Skyscan, UK). 3D reconstruction from micro-CT datasets was performed using NRecon, Data Viewer, CTAn, and CTVol software (Bruker, Belgium). Next, a cylindrical region (3×1 mm) within the defect was selected as the volume of interest (VOI). Bone volume (BV), percentage bone volume (bone volume/total volume, BV/TV), and bone surface/volume ratio (BS/BV) were evaluated from the 3D reconstructed images.

2.15.3 | Histological examination

Fixed skull samples were treated by decalcifying solution for 2 weeks. The samples were subsequently dehydrated, embedded in paraffin wax. Consecutive 4 μm-thick horizontal sections were obtained from the defect area. To investigate new bone formation, hematoxylin and eosin (H&E) staining (Servicebio, GP1031, China) and Masson staining (Servicebio, GP1032, China) were performed on samples obtained 6 weeks after injection of GelMA. Images were captured using an upright microscope (Olympus BX60, Japan).

2.15.4 | Immunohistochemistry

After dewaxing and dehydrating, the sections were treated with EDTA antigen retrieval (Solarbio, C1034, Beijing) for 10 min at 37°C. Then, 5% goat serum (ZSGB-BIO) was used to block non-specific binding. The primary antibodies including anti-YAP (Proteintech), anti-TAZ (Abcam), anti-TEAD4 (Abcam), anti-OCN (Proteintech) and added to sections at 4°C overnight. After rinsing three times with PBS, the sections were incubated with corresponding horseradish peroxidase-conjugated secondary antibodies (ZB-2306, ZSGB-Bio, China) at room temperature for 1 h. DAB kit (ZLI-9018, ZSGB Bio, China) was used to coloration. After rinsing with tap water, hematoxylin was added to the sections and then soaked into tap water. The samples were observed under an upright microscopy (Olympus BX60).

2.16 | Statistical analysis

SPSS25 software was used for statistical analysis. Experiments were repeated triplicate independently. All in vivo and in vitro data were presented as means ± standard deviation (SD) or standard error of means. Statistical analysis was conducted by t tests or one-way analysis of variance (ANOVA). Differences were considered statistically significant at $p < 0.05$.
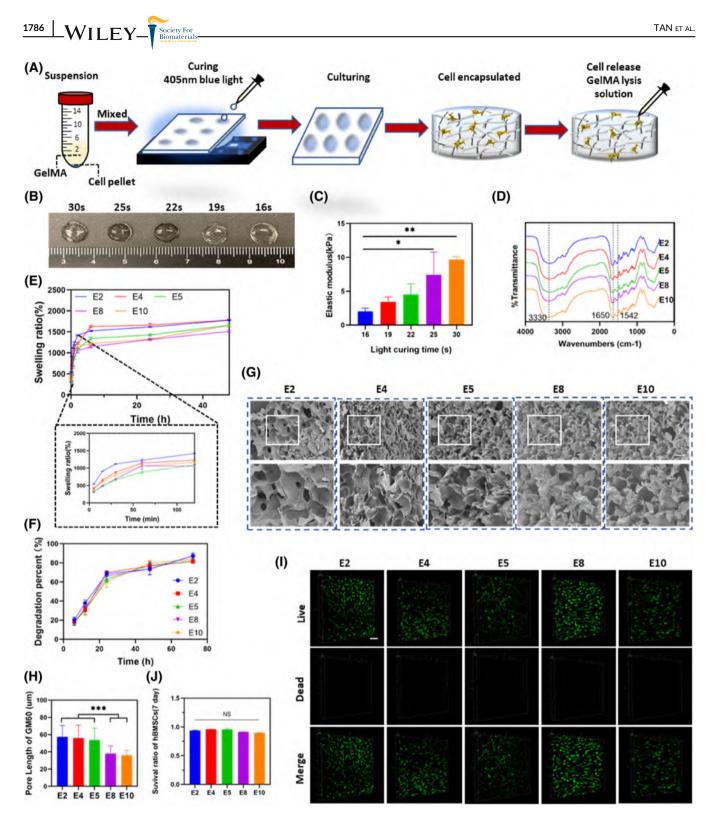
3 | RESULTS

3.1 | Physical and chemical properties of GelMA

GelMA is widely used in tissue engineering due to the excellent biocompatibility and tunable physical properties. Thus, GelMA was used in the present study to build the culture environment of different elastic modulus. hBMSCs were evenly dispersed in GelMA and added into the dish. After light curing for different seconds, hBMSCs were encapsulated and cultured. A GelMA lysis buffer was used if collection of hBMSCs were needed (Figure 1A). The curing times was set to be 16, 19, 22, 25, and 30 s. Empty GelMA was semi-transparent in all groups (Figure 1B). The elastic modulus of GM60 increased gradually with the increase of curing time. And we set five groups according its elastic modulus as E2 group ($\sim$2 kPa), E4 group ($\sim$4 kPa), E5 group ($\sim$5 kPa), E8 group ($\sim$8 kPa), and E10 group ($\sim$10 kPa) respectively (Figure 1C). FT-IR showed that the elastic modulus did not influence the absorbance peaks of GM60 (Figure 1D). The swelling ratio and biodegradability of GM60 did not differ significantly among the five groups within 48 h and 72 h (Figure 1E,F), indicating that the elastic modulus does not affect the swelling and degradation properties of GelMA.

SEM showed that the pores of GelMA were largest in E2 and smallest in E10 because of the increased degree of cross-linking (Figure 1G,H). Live/dead staining showed that the viability rate did not differ significantly among the five groups, indicating that all the five groups had good biocompatibility (Figure 1I,J).

3.2 | Effect of elastic modulus on hBMSCs differentiation

We then analyzed how the GelMA of different elastic modulus affect osteogenic differentiation. qRT-PCR results showed that expression of OPG decreased in E2 compared to E5, E8 or E10, while the expression of MMP9 was increased in E2 compared to E8 or E10 (Figure 2A). YAP and TAZ are key effector proteins in the cellular response to mechanical signals.[27] TEA domain family member (TEAD) transcription factors are the main partners of YAP and TAZ.[28] OPG blocks the differentiation of osteoclasts and OCN is an osteogenic marker gene.[29,30] We then analyzed the effect of elastic modulus on the expression of YAP, TAZ, TEAD, OPG and OCN. qRT-PCR and

FIGURE 1 Physical, chemical, and biocompatible properties of GelMA. (A) Schematic illustration of constructing 3D GelMA model. (B) Images of GelMA for cured 16 s, 19 s, 22 s, 25 s, and 30s. (C) Elastic modulus of GelMA for cured 16 s, 19 s, 22 s, 25 s, and 30s. (D) FTIR of GelMA in E2, E4, E5, E8, and E10. (E) Swelling ratio of GelMA in E2, E4, E5, E8, and E10. (F) Degradation of GelMA in E2, E4, E5, E8, and E10. (G) Upper panel: SEM images of GelMA in E2, E4, E5, E8, and E10; scale bar, 50 μm. Lower panel: higher magnification of the boxed area in the upper panel. (H) Quantification of pore length of GelMA in E2, E4, E5, E8, and E10. (I) Live/dead staining of hBMSCs in GelMA in E2, E4, E5, E8, and E10; scale bar, 200 μm. (J) Survival rate of hBMSCs did not differ among E2, E4, E5, E8, and E10. ($n = 3$ per group. All ata were presented as means ± SD; *$p < .05$, **$p < .01$, ***$p < .001$, NS: no significance).
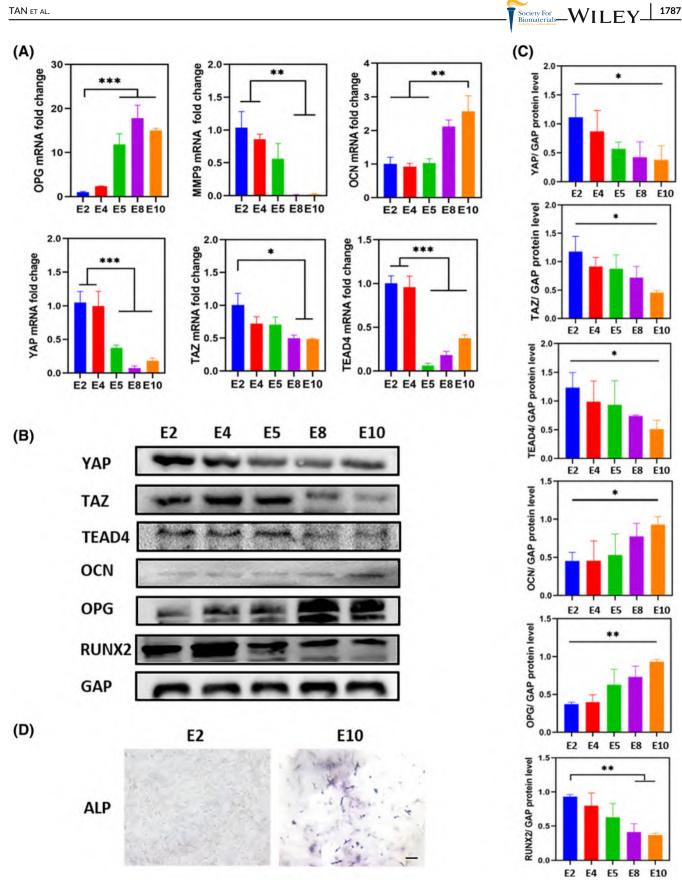
FIGURE 2 Differentiation of hBMSCs in GelMA. (A) mRNA levels of OPG, MMP9, OCN, YAP, TAZ, and TEAD4 in E2, E4, E5, E8, and E10. (B) Western blots of YAP, TAZ, TEAD4, OCN, OPG, RUNX2 and GAP in E2, E4, E5, E8, and E10. (C) Protein quantification of YAP, TAZ, TEAD4, OCN, OPG and RUNX2. (D) Representative. images of ALP staining of hBMSCs cultured in E2 or E10 in 7 days. Scale bar = 100 μm ($n = 3$ per group. All data were presented as means ± SD; $*p < .05$, $**p < .01$, $***p < .001$).
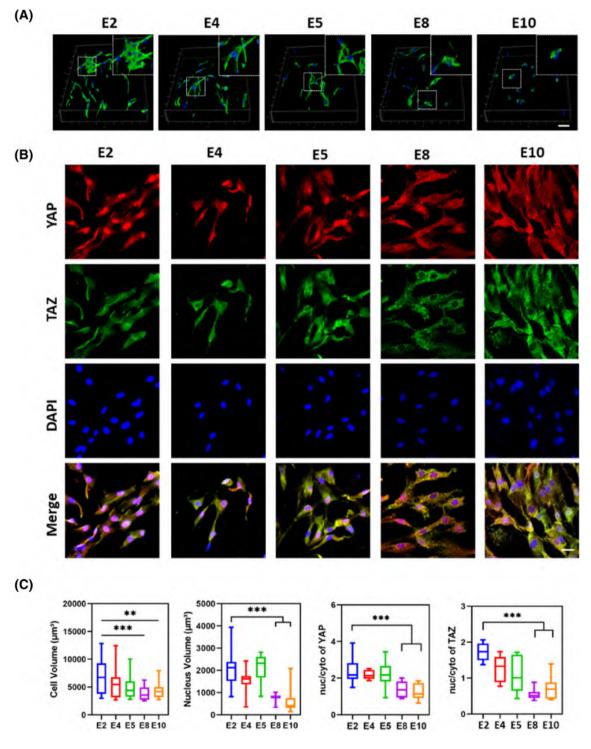
western blot showed that YAP, TAZ, and TEAD expression was the highest in E2, OPG and OCN decreased in E2 compared to E10 (Figure 2A-C). These results showed that high-elastic-modulus hydrogel (E10) promoted osteogenesis of hBMSCs. However, RUNX2 expressed higher in low-elastic-modulus hydrogel (E2 and E4, Figure 2B,C). Since RUNX2 was the marker of the early stage in osteogenesis. OCN expressed at the onset of mineralization during development of the osteogenesis and reaches peak levels during mineralization. OPG inhibited osteoclast differentiation from precursor cells. RUNX2, OCN, OPG expressed differently in different stage of bone formation.[31–33] ALP stain also showed that hBMSCs in E10 had stronger ALP activity than E2 (Figure 2D). These data showed that
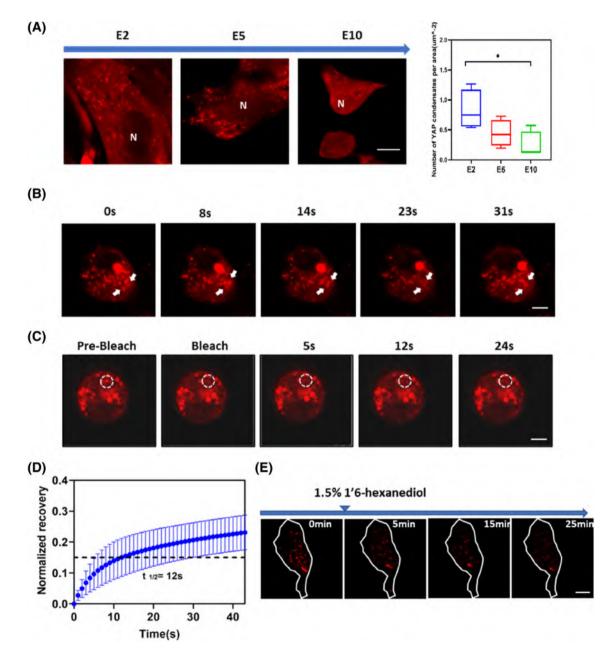

FIGURE 3 Morphology of hBMSCs and YAP / TAZ nuclear translocation. (A) Cytoskeleton stain of hBMSCs in E2, E4, E5, E8, and E10. Scale bar, 50 μm. (B) Immunofluorescence of YAP/TAZ translocation. Scale bar, 25 μm. (C) Quantification of cell volume, nuclei volume, nuc / cyto ratio of YAP and TAZ. ($n = 3$ per group. All data were presented as means ± SD; **$p < .01$, ***$p < .001$).
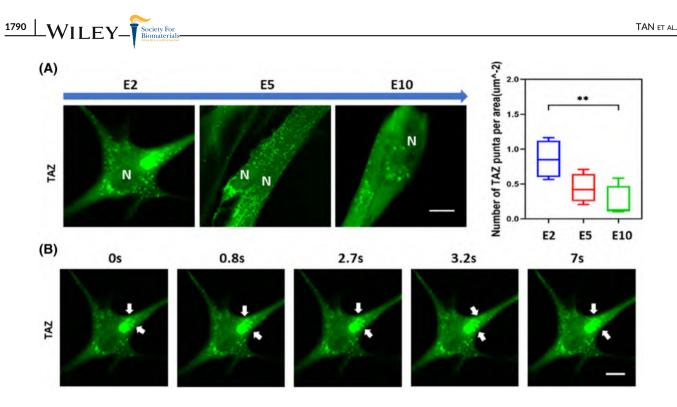
high-elastic-modulus GelMA decreased the expression of YAP and TAZ, yet promoted the hBMSCs differentiation to mature osteoblast.

3.3 | Morphology of hBMSCs and YAP/TAZ nuclear translocation

osteoclast differentiation from precursor that F-actin (green) was more integrated in E2, E4 and E5, sustaining the branched shape of hBMSCs. In E8 and E10, hBMSCs were spherical (Figure 3A).

Quantification of cell and nuclei volume indicated that hBMSCs spread in GelMA of low elastic modulus (E2, E4, and E5), but compressed in GelMA of high elastic modulus (E8 and E10) (Figure 3C). Caliari et al. reported that YAP and TAZ translocated into the nucleus when cells were cultured in surface of stiffer hydrogels, and translocated into nucleus in 3D soft matrix.[34] In our 3D GelMA model, YAP and TAZ translocated to the nucleus in E2, E4, and E5, but mainly distributed in cytoplasm in E8 and E10 (Figure 3B). The nuc / cyto ratios of YAP and TAZ in E2 were significantly higher than E8 and E10 (Figure 3C).

FIGURE 4 LLPS of YAP occurred in GelMA of low elastic modulus. (A) Live-cell imaging of YAP condensates in E2, E5, and E10. N, nucleus. Scale bar, 10 μm. The number of YAP condensates normalized to cell area. (B) Fusion of YAP condensates in E2 (white arrow). Scale bar, 5 μm. (C) FRAP recovery of YAP condensates. White cycle indicates photobleaching area. Scale bar, 5 μm. (D) FRAP recovery curve of YAP condensates. Data are presented as means and standard error of means ($t_{1/2} = 12$ s). (E) Live-cell images of hydrophobic-sensitive phase-separation of YAP condensates in 1,6-hexanediol-treated hBMSCs. Scale bar, 5 μm. ($n = 4$ per group. All data were presented as means ± SD except for (D); *$p < .05$).

FIGURE 5 LLPS of TAZ occurred in GelMA. (A) Live-cell imaging of TAZ condensates in E2, E5, and E10. N, nucleus. Scale bar, 25 μm. The number of TAZ condensates normalized to cell area. (B) Fusion of TAZ condensates in E2 (white arrow). Scale bar, 25 μm. (n = 4 per group. All data were presented as means ± SD; **p < .01).

3.4 | GelMA of low elastic modulus drive YAP phase separation

According to the analysis of ANCHOR2 and IUPred2 algorithms, more than 90% of YAP amino acid sequences had disorder scores of >0.5 and had an intrinsic phase-separation ability in our 3D GelMA model, hBMSCs were transfected with an mCherry-YAP plasmid in E2, E5, and E10. Live-cell images showed that YAP condensates possessed high sphericity and fusion behavior. Furthermore, the number of YAP condensates per square micron in E2 was significantly higher than in E5 and E10 (Figure 4A). Time-lapse imaging showed fusion process of YAP condensates in E2 group (Figure 4B). The fluorescence intensity of YAP condensates also recovered gradually after photobleaching ($t_{1/2}$ = 12 s; Figure 4C,D). 1,6-Hexanediol interferes with hydrophobic protein–protein interactions, depolymerizing protein condensates and dissociating proteins from chromatin.[35] In E2, YAP condensates were sensitive to 1,6-Hexanediol and dispersed gradually within 25 min (Figure 4E). These data showed that YAP condensates represented a liquid phase formed by LLPS and influenced by the elastic modulus of GelMA.

3.5 | GelMA of low elastic modulus drives TAZ phase separation

According to the analysis of ANCHOR2 and IUPred2 algorithms, the full-length protein of TAZ also contained multiple IDRs. We

transfected equal amounts of EGFP-TAZ plasmids into hBMSCs in E2, E5, and E10. Live-cell imaging showed that TAZ was more apt to congregate and form condensates in E2, similar to YAP condensates. Also, the number of TAZ condensates per square micron was higher in E2 than in E5 and E10 (Figure 5A). Time-lapse imaging of TAZ condensates showed the fusion process (Figure 5B). Therefore, GelMA of low elastic modulus promoted TAZ LLPS.
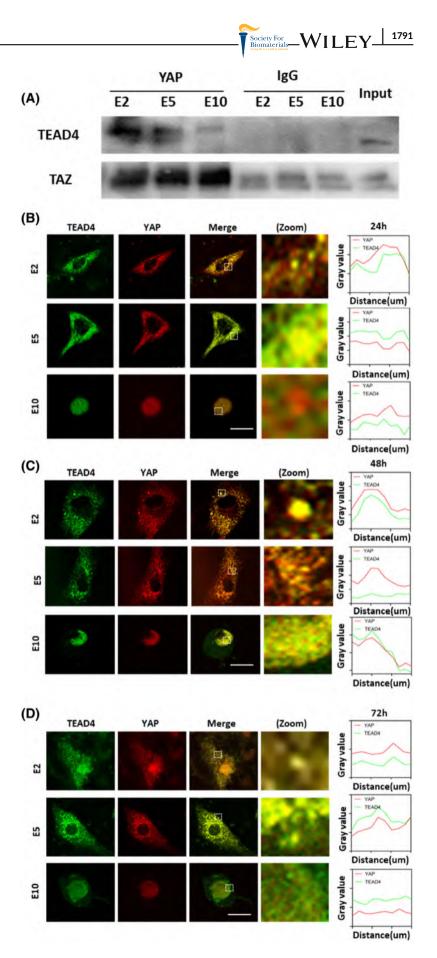
3.6 | YAP condensates compartmentalize TEAD4

On the basis of endogenous interaction of YAP and TEAD4 (Figure 6A), we analyzed if TEAD4 was associated with YAP LLPS in GelMA. Live-cell imaging showed that YAP colocalized with TEAD4, and we observed fusion events of TEAD4 and YAP in E2 at 24, 48, and 72 h. Although the puncta of YAP and TEAD4 can be spotted in E5 at 48 and 72 h, no obvious condensates were spotted in E10 and the intensity patterns of TEAD4 deviated from that of YAP in E10 (Figure 6B–D).

3.7 | YAP condensates compartmentalize TAZ but without RUNX2

To identify other components of YAP condensates, we investigated TAZ and RUNX2, which may synergistically regulate gene expression.[23,36] We also observed endogenous interaction of YAP and TAZ

FIGURE 6 YAP condensates contain TEAD4. (A) Co-IP of YAP and TEAD4, YAP and TAZ. Live-cell imaging of TEAD4 (green) and YAP (red) condensates after co-transfection of EGFP-TEAD4 and mCherry-YAP plasmids at 24 h (A), 48 h (B), and 72 h (C). Scale bar, 25 μm. Zoom, gher magnification image of the white boxed area. Line plot of colocalization of YAP and TEAD4 condensates was shown on the right panel. (n = 3 per group).
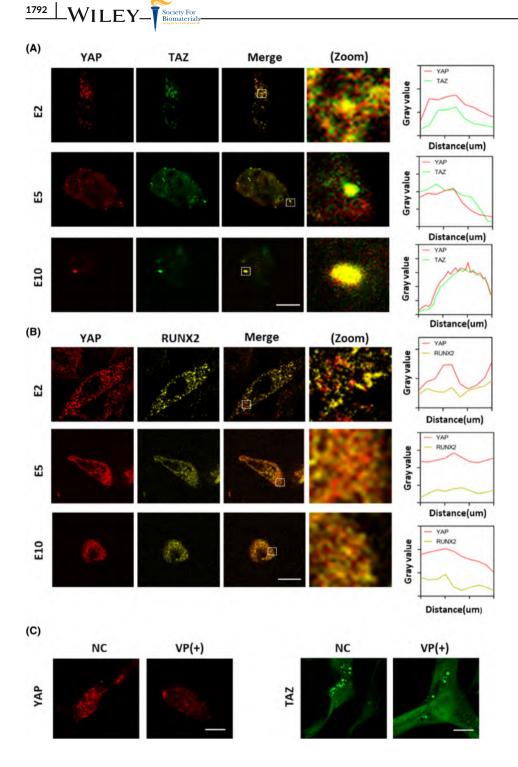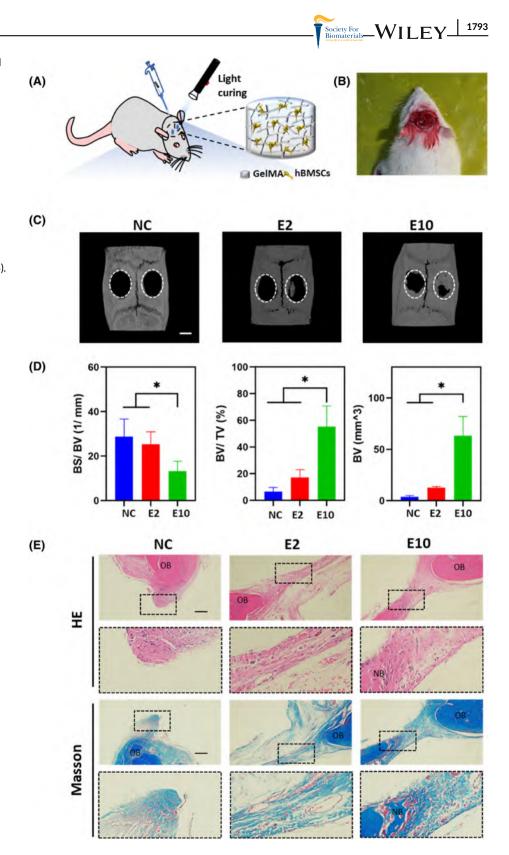
FIGURE 7 YAP condensates contain TAZ but not RUNX2. (A) Live-cell images of YAP (red) and TAZ (green) condensates at 48 h after transfection of mCherry-YAP and GFP-TAZ plasmids. Zoom represents a zoomed-in view of the white box. Scale bar, 25 μm. Line plot of colocalization of YAP and TAZ condensates was shown on the right panel. (B) Live-cell images of YAP (red) and RUNX2 (yellow) condensates at 48 h after transfection of mCherry-YAP and YFP-RUNX2 plasmids. Zoom represents a zoomed-in view of the white box. Scale bar, 25 μm. Line plot of colocalization of YAP and RUNX2 condensates was shown on the right panel. (C) Live-cell images of YAP (red) and TAZ (green) condensates after adding VP for 48 h in E2. Scale bar, 25 μm. ($n = 3$ per group).

(Figure 6A). Live-cell imaging showed that condensates formed and intensity pattern of YAP and TAZ were consistent in E2, E5 and E10 (Figure 7A). When YAP and RUNX2 were co-transfected into hBMSCs, separate puncta of YAP and RUNX2 were observed in E2, E5 and E10, but the intensity pattern did not match between YAP and RUNX2 (Figure 7B). We also used VP, a YAP inhibitor, to specifically disrupt YAP-TEAD interaction.[37] We observed that LLPS of YAP/TAZ attenuated when hBMSCs were incubated with VP for 48 h in E2 (Figure 7C). These data suggested that YAP condensates recruited TEAD and TAZ, but not RUNX2, when cultured in GelMA of low elastic modulus (E2).

3.8 | GelMA of high elastic modulus promotes osteogenesis in vivo

We established a rat calvarial defect model (Figure 8A,B). At 6 weeks after surgery, no obvious inflammation or necrosis was observed in E2, E10, and NC, indicating GelMA has good bioactivity and exhibits biosafety. micro-CT analysis showed that more neo-bone formation was observed in E10 compared with E2 (Figure 8C). The BS/BV ratio were decreased in E10. The BV/TV ratio and the BV values were increased in E10 compared to E2 and NC (Figure 8D). Bone analysis by H&E staining showed that the rat defect site in E10 had
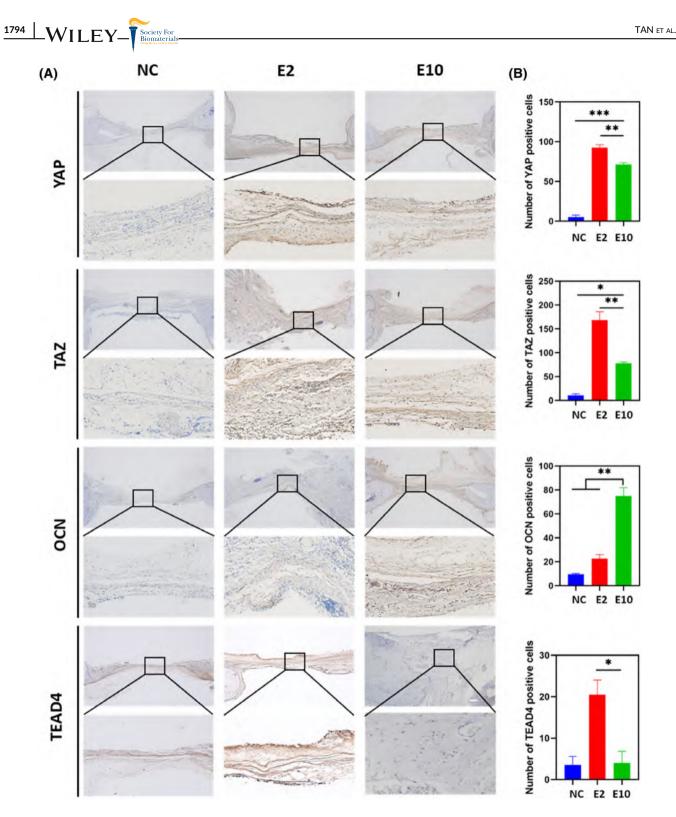
FIGURE 8 GelMA of E10 promoted bone formation in vivo. (A) and (B) Schematic of rat calvarial defect model. GelMA encapsulated hBMSCs (E2, E10, and NC) implanted into defect sites for 6 weeks. (C) Representative micro-CT images of E10, E2, and NC. Scale bar, 2 mm. (D) New bone formation in the calvarial defect area quantified as BS/ BV, BV/TV, and BV values. (E) H&E and Masson staining of regenerated bone in rats. NB, neo-bone (black dotted box); OB, old bone. Scale bar, 100 μm. ($n = 3$ per group. All data were presented as means ± SD; *$p < .05$).

significantly increased bone formation compared to E2 and NC. Masson staining indicated more collagen fibers in E10 than E2 (Figure 8E). Immunohistochemistry stain showed that YAP, TAZ and TEAD4 were increased in E2 compared to E10 and NC, whereas OCN expression was increased in E10 (Figure 9A,B). Therefore, GelMA of high elastic modulus induced more bone formation compared with that of low elastic modulus.

4 | DISCUSSION

In the present study, we constructed 3D GelMA to investigated how the elastic modulus of hydrogel affect osteogenic differentiation. hBMSCs spread and branched in GelMA. YAP expression increased in GelMA of low elastic modulus. Importantly, YAP self-congregated in GelMA of low elastic modulus (E2), but not in that of high elastic

FIGURE 9 Immunohistochemistry staining of YAP, TAZ, OCN and TEAD4. (A) Immunohistochemistry stain of YAP, TAZ, OCN and TEAD4 in E10, E2 and NC. Scale bar, 200 μm. (B) Quantification of YAP, TAZ, OCN and TEAD4 positive cells number in E10, E2 and NC. ($n = 3$ per group. All data were presented as means ± SD; *$p < .05$, **$p < .01$, ***$p < .001$).

modulus (E10). This is possibly due to the increased concentration of YAP. This is consistent with condensation polymerization and concentration dependence theories.[12,38] YAP assembles into condensates in the presence of crowding agents (e.g., PEG-8000, Ficoll, and Dextran); however, the underlying mechanism is unclear. It is possible that crowding agents decrease the available space, thus increasing the intracellular biomacromolecule concentration.[39] This hypothesis is in accordance with the increased LLPS of YAP in E2.

LLPS occurs under certain conditions.[11] LLPS dynamically regulates physiological reactions, increases local protein concentrations,
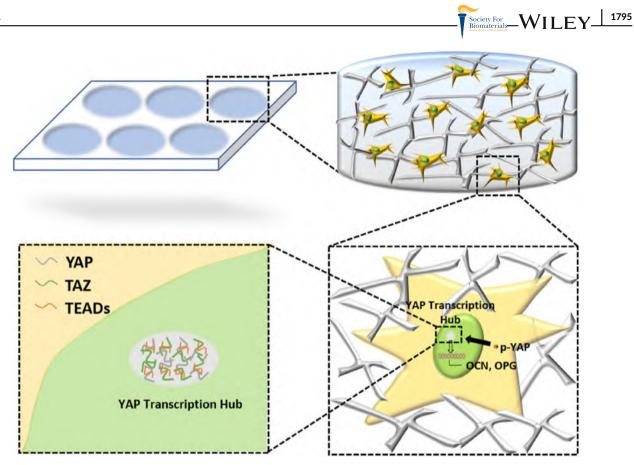
FIGURE 10 A schematic illustration of the YAP LLPS in GelMA. The underlying mechanism of YAP LLPS mediated bone regeneration.

and decreases molecular motion by enhancing viscoelasticity.[13] YAP, a pivotal protein in the Hippo pathway, is implicated in mechanical signal transduction. YAP selectively binds several transcription factors, thus influencing cell fate.[27] YAP contains different domains, including TB, WW, CC, and TA domains.[40,41] The TA domain of other transcription cofactors mediates phase separation,[42] and that in YAP is responsible for reversible phase separation under hyperosmotic stress.[18,20] The CC and WW domains are necessary for YAP LLPS and binding to transcription factors to activate gene transcription.[19] For example, YAP.ErbB4 complex formation is mediated by the first WW domain of YAP.[43] p73 is also associated with the WW domain of YAP.[44] Therefore, the YAP WW domain is important for its binding to transcription factors and activating target gene expression.[45] We did not identify the YAP domain responsible for LLPS, but the TB domain which mediates the binding of YAP and TEAD is the possible candidate.

In our 3D GelMA models, hBMSCs was more apt to osteogenic differentiation in high-elastic-modulus (∼10 kPa) hydrogel compared to low-elastic-modulus (∼2 kPa) hydrogel. Major et.al constructed a GelMA hydrogel with a continuous stiffness gradient ranging from 5 to 38 kPa. Even though in hard (∼30 kPa) 3D GelMA hydrogel, adipose-derived stem cells inclined to adipogenic differentiation. In soft (∼8 kPa) 3D GelMA hydrogel, adipose-derived stem cells apt to osteogenic differentiation.[46] This is partly consistent with our results that a relatively soft (∼10 kPa) GelMA hydrogel promoted hBMSCs osteogenesis. Further, in our study, the expression of YAP was increased in the low-elastic-modulus GelMA (∼2 kPa). Caliari et. al found that the nuclear

location of YAP/ TAZ increased atop 2D hydrogel surface(∼20 kPa) compared to low stiffness hydrogel surface(∼1 kPa). But when stem cells encapsulated in 3D hydrogels, the nuc/ cyto ratio of YAP/TAZ remained highest (∼1.5) in low stiffness hydrogel (∼1 kPa) compared to high stiffness hydrogel (∼20 kPa).[34] It was also in accordance with our findings that YAP translocated into nuclear when cells were encapsulated in soft hydrogel (∼2 kPa). The nuc/ cyto ratio of YAP and the cellular volume decreased with the increase of stiffness in 3D hydrogel.

YAP was found to play opposing role during different stages of osteoblast differentiation. Deletion of YAP and TAZ from progenitor cells increased osteoblast differentiation, deletion of YAP and TAZ from mature osteoblasts and osteocytes reduced osteoblast number and bone formation in vitro. YAP and TAZ were found to suppress the activity of RUNX2 in osteoblast progenitor cells.[47] Moreover, a YAP inhibitor was shown to promote osteogenic differentiation by against TEADs-inhibited RUNX2 transcription.[48] However, high-curvature environments promoted osteogenic differentiation through YAP, and inhibition of YAP decreased the osteogenic differentiation of pre-osteoblasts.[49] The discrepancy may be due to use of different cell types, stimuli, and co-activators. YAP did not recruit RUNX2, the critical transcription factor regulating osteoblast differentiation, may account for the inferior performance of GelMA with low elastic modulus.

GelMA has been used in tissue engineering scaffolds based on its biocompatibility, biodegradability, active side chains, high hydrophilicity, and stable physical and chemical properties.[50] Modifying the polypeptide or arginine-glycine-aspartate sequence of gelatin can enhance cell

adhesion, differentiation, and proliferation.[51,52] For example, an osteogenic polypeptide hydrogel was created by co-crosslinking photo-cross-linked GelMA with photo-cross-linkable osteogenic growth peptides using ultraviolet radiation. This novel material significantly accelerated bone formation in vivo and in vitro.[53] In this study, GelMA cross-linking increased with the increasing curing time, altering pore size and elasticity. Although curing time did not affect functional groups, swelling ratio, or biodegradability, it regulated stem cell differentiation fate. Thus, the elastic modulus of GelMA should be considered in further application.

In summary, in our study, GelMA of high elastic modulus promoted hBMSCs osteogenic differentiation by regulating YAP LLPS. Specifically, YAP condensates recruited TAZ and TEAD4, but not RUNX2, regulating OCN and OPG expression (Figure 10). YAP phase separation may be a new entry point to alter the course of bone formation. Regulators of elastic modulus or YAP LLPS may be applied in bone defects or other diseases.

5 | CONCLUSIONS

In this study, we found that the expression of YAP, TAZ and TEAD4 was increased in the low-elastic-modulus GelMA. The expression of osteogenic markers was inhibited in the low-elastic-modulus GelMA. Furthermore, YAP assembled LLPS and recruit TAZ and TEAD4, but not RUNX2 into the condensates in low-elastic-modulus GelMA. In vivo, we also found that hBMSCs in high-elastic-modulus GelMA was more apt to form new bone. We can infer GelMA of high-elastic-modulus may promote osteogenic differentiation of hBMSCs via LLPS of YAP. This study provides new insight into the mechanism of osteogenic differentiation. Reagents regulate the elastic modulus of substrate or LLPS may be applied to promote bone regeneration.

AUTHOR CONTRIBUTIONS

Kuang Tan: Conception and design, Methodology, Data collection and analysis, Investigation, manuscript writing. **Qiaolin Yang, Yineng Han, Ziyao Zhuang, Yi Zhao:** Methodology, Data curation, Formal analysis. **KunYao Guo, Anqi Tan:** Methodology, Data curation. **Yunfei Zheng:** Conception and design, Methodology, Investigation, Manuscript writing, Final approval of manuscript. **Weiran Li:** Conception and design, financial support and final approval of manuscript.

ACKNOWLEDGMENTS

FUNDING INFORMATION

CONFLICT OF INTEREST STATEMENT

The author(s) declare that they have no known competing financial interests or personal relationships that may influence the work reported in this article.

DATA AVAILABILITY STATEMENT

All data on this study are available within this publication or can be provided upon request.

CONSENT FOR PUBLICATION

All authors have read and approved the publication of the manuscript.

ORCID
Kuang Tan https://orcid.org/0000-0002-6889-1108

Weiran Li https://orcid.org/0000-0001-9895-1143

REFERENCES

1. Yu X, Huang Y, Li W. Correlation between alveolar cleft morphology and the outcome of secondary alveolar bone grafting for unilateral cleft lip and palate. *BMC Oral Health*. 2022;22(1):251.
2. Hagar MN, Yazid F, Luchman NA, Ariffin SHZ, Wahab RMA. Comparative evaluation of osteogenic differentiation potential of stem cells derived from dental pulp and exfoliated deciduous teeth cultured over granular hydroxyapatite based scaffold. *BMC Oral Health*. 2021; 21(1):263.
3. Tögel F, Westenfelder C. Adult bone marrow-derived stem cells for organ regeneration and repair. *Dev Dyn*. 2010;236(12):3321-3331.
4. Conti L, Pollard SM, Gorba T, et al. Niche-independent symmetrical self-renewal of a mammalian tissue stem cell. *PLoS Biol*. 2005;3(9):e283.
5. Yang C, Tibbitt MW, Basta L, Anseth KS. Mechanical memory and dosing influence stem cell fate. *Nat Mater*. 2014;13(6):645-652.
6. Engler AJ, Sen S, Sweeney HL, Discher DE. Matrix elasticity directs stem cell lineage specification. *Cell*. 2006;126(4):677-689.
7. Chaudhuri O, Gu L, Klumpers D, et al. Hydrogels with tunable stress relaxation regulate stem cell fate and activity. *Nat Mater*. 2016;15(3): 326-334.
8. Rehmann MS, Luna JI, Maverakis E, Kloxin AM. Tuning microenvironment modulus and biochemical composition promotes human mesenchymal stem cell tenogenic differentiation. *J Biomed Mater Res A*. 2016;104(5):1162-1174.
9. Mcswiggen DT, Hansen AS, Teves SS, Marie-Nelly H, Darzacq X. Evidence for DNA-mediated nuclear compartmentalization distinct from phase separation. *eLife Sciences*. 2019;8:8.
10. Berg OG, Winter RB, Hippel P. Diffusion-driven mechanisms of protein translocation on nucleic acids. 1. Models and theory. *Biochemistry*. 1981;20(24):6929-6948.
11. Peng A, Weber SC. Evidence for and against liquid-liquid phase separation in the nucleus. *Non-Coding RNA*. 2019;5(4):50.
12. Li P, Banjade S, Cheng HC, et al. Phase transitions in the assembly of multivalent signalling proteins. *Nature*. 2012;483(7389):336-340.
13. Banani SF, Rice AM, Peeples WB, et al. Compositional control of phase-separated cellular bodies. *Cell*. 2016;166(3):651-663.
14. Martin EW, Holehouse AS. Intrinsically disordered protein regions and phase separation: sequence determinants of assembly or lack thereof. *Emerg Top Life Sci*. 2020;4(3):307-329.
15. Zhao B, Lei QY, Guan KL. The hippo-YAP pathway: new connections between regulation of organ size and cancer. *Curr Opin Cell Biol*. 2008;20(6):638-646.
16. Heng BC, Zhang X, Aubel D, et al. Role of YAP/TAZ in cell lineage fate determination and related signaling pathways. *Front Cell Dev Biol*. 2020;8:735.
17. Yu M, Peng Z, Qin M, et al. Interferon-gamma induces tumor resistance to anti-PD-1 immunotherapy by promoting YAP phase separation. *Mol Cell*. 2021;81(6):1216-1230.e9.
18. Cai D, Feliciano D, Dong P, et al. Phase separation of YAP reorganizes genome topology for long-term YAP target gene expression. *Nat Cell Biol*. 2019;21(12):1578-1589.

19. Wu T, Lu Y, Gutman O, Lu H, Luo K. Phase separation of TAZ compartmentalizes the transcription machinery to promote gene expression. *Nat Cell Biol*. 2022;22(4):453-464.

20. Franklin JM, Guan KL. YAP/TAZ phase separation for transcription. *Nat Cell Biol*. 2020;22(4):357-358.

21. Seo E, Basu-Roy U, Gunaratne PH, et al. SOX2 regulates YAP1 to maintain stemness and determine cell fate in the osteo-adipo lineage. *Cell Rep*. 2013;3(6):2075-2087.

22. Pan JX, Xiong L, Zhao K, et al. YAP promotes osteogenesis and suppresses adipogenic differentiation by regulating β-catenin signaling. *Bone Res*. 2018;1(6):18.

23. Zhao L, Guan H, Song C, et al. YAP1 is essential for osteoclastogenesis through a TEADs-dependent mechanism. *Bone*. 2018;110:177-186.

24. Passaniti A, Brusgard JL, Qiao Y, Sudol M, Finch-Edmonson M. Roles of RUNX in hippo pathway signaling. *Adv Exp Med Bio*. 2017;962:435-448.

25. Lim B, Park JL, Kim HJ, et al. Integrative genomics analysis reveals the multilevel dysregulation and oncogenic characteristics of TEAD4 in gastric cancer. *Carcinogenesis*. 2014;35(5):1020-1027.

26. Plouffe SW, Lin KC, Moore JL III. The hippo pathway effector proteins YAP and TAZ have both distinct and overlapping functions in the cell. *J Biol Chem*. 2018;13(28):11230-11240.

27. Halder G, Dupont S, Piccolo S. Transduction of mechanical and cytoskeletal cues by YAP and TAZ. *Nat Rev Mol Cell Biol*. 2012;13(9):591-600.

28. Zhao B, Li L, Lei Q, Guan KL. The hippo-YAP pathway in organ size control and tumorigenesis: an updated version. *Genes Dev*. 2010;9:24-874.

29. Cao T, Heng BC, Ye CP, et al. Osteogenic differentiation within intact human embryoid bodies result in a marked increase in osteocalcin secretion after 12 days of in vitro culture, and formation of morphologically distinct nodule-like structures. *Tissue Cell*. 2005;37(4):325-334.

30. Hofbauer LC, Kühne C, Viereck V. The OPG/RANKL/RANK system in metabolic bone diseases [review]. *J Musculoskelet Neuronal Interact*. 2004;4(3):268-275.

31. Beddington R. The atlas of mouse development. *Trends Genet*. 1993;9(1):32.

32. Jane B, Lian GS, Stein JL, Stein A. Osteocalcin gene promoter: unlocking the secrets for regulation of osteoblast growth and differentiation. *J Cell Biochem*. 1998;72:62-72.

33. Simonet WS, Lacey DL, Dunstan CR, Kelley MC, Boyle WJ. Osteoprotegerin: a novel secreted protein involved in the regulation of bone density. *Cell*. 1997;89(2):309-319.

34. Caliari SR, Vega SL, Kwon M, Soulas EM, Burdick JA. Dimensionality and spreading influence MSC YAP/TAZ signaling in hydrogel environments. *Biomaterials*. 2016;103:314-323.

35. Liu X, Jiang S, Ma L, et al. Time-dependent effect of 1,6-hexanediol on biomolecular condensates and 3D chromatin organization. *Genome Biol*. 2021;22(1):230.

36. Lin X, Yang H, Wang L, et al. AP2a enhanced the osteogenic differentiation of mesenchymal stem cells by inhibiting the formation of YAP/RUNX2 complex and BARX1 transcription. *Cell Prolif*. 2019;52(1):e12522.

37. Pan W, Wang Q, Zhang Y, et al. Verteporfin can reverse the paclitaxel resistance induced by YAP over-expression in HCT-8/T cells without Photoactivation through inhibiting YAP expression. *Cell Physiol Biochem*. 2016;39(2):481-490.

38. Cohen RJ, Benedek GB. Equilibrium and kinetic theory of polymerization and the sol-gel transition. *J Phys Chem*. 2002;86(19):3696-3714.

39. Xu Y, Qi R, Zhu H, et al. Liquid-liquid phase-separated systems from reversible gel-sol transition of protein microgels. *Adv Mater*. 2021;33(33):e2008670.

40. Claire W, Abhishek U, Francesca G, Ian E, Makoto F-S. Structural features and ligand binding properties of tandem WW domains from YAP and TAZ, nuclear effectors of the hippo pathway. *Biochemistry*. 2011;50(16):3300-3309.

41. Kaan H, Chan SW, Tan S, et al. Crystal structure of TAZ-TEAD complex reveals a distinct interaction mode from that of YAP-TEAD complex. *Sci Rep*. 2017;7(1):2035.

42. Boija A, Klein IA, Sabari BR, Dall'Agnese A, Young RA. Transcription factors activate genes through the phase-separation capacity of their activation domains. *Cell*. 2018;175(7):1842-1855.e16.

43. Komuro A, Nagai M, Navin NE, Sudol M. WW domain-containing protein YAP associates with ErbB-4 and acts as a Co-transcriptional activator for the carboxyl-terminal fragment of ErbB-4 that Translocates to the nucleus. *J Biol Chem*. 2003;278(35):33334-33341.

44. Strano S, Monti O, Baccarini A, Sudol M, Sacchi A, Blandino G. Physical interaction with yes-associated protein enhances p73 transcriptional activity. *Eur J Cancer*. 2001;37(Supplement 6):S279.

45. Totaro A, Panciera T, Piccolo S. YAP/TAZ upstream signals and downstream responses. *Nat Cell Biol*. 2018;20(8):888-899.

46. Major LG, Holle AW, Young JL, et al. Volume adaptation controls stem cell Mechanotransduction. *ACS Appl Mater Interfaces*. 2019;11(49):45520-45530.

47. Xiong J, Almeida M, O'Brien CA. The YAP/TAZ transcriptional co-activators have opposing effects at different stages of osteoblast differentiation. *Bone*. 2018;112:1-9.

48. Suo J, Feng X, Li J, et al. VGLL4 promotes osteoblast differentiation by antagonizing TEADs-inhibited Runx2 transcription. *Sci Adv*. 2020;6(43).

49. Liu Y, Yang Q, Wang Y, et al. Metallic scaffold with Micron-scale geometrical cues promotes Osteogenesis and angiogenesis via the ROCK/myosin/YAP pathway. *ACS Biomater Sci Eng*. 2022;8(8):3498-3514.

50. Ansari S, Sarrion P, Hasani-Sadrabadi MM, Aghaloo T, Wu BM, Moshaverinia A. Regulation of the fate of dental-derived mesenchymal stem cells using engineered alginate-GelMA hydrogels. *J Biomed Mater Res A*. 2017;105(11):2957-2967.

51. Jiang N, Wang Y, Yin Y-X, et al. bFGF and poly-RGD cooperatively establish biointerface for stem cell adhesion, proliferation, and differentiation. *Adv Mater Interfaces*. 2018;5(7):1700702.

52. Liu Y, Chan-Park MB. A biomimetic hydrogel based on methacrylated dextran-graft-lysine and gelatin for 3D smooth muscle cell culture. *Biomaterials*. 2010;31(6):1158-1170.

53. Qiao Y, Liu X, Zhou X, et al. Gelatin Templated polypeptide Co-cross-linked hydrogel for bone regeneration. *Adv Healthc Mater*. 2020;9(1):1901239.